Journal of Power Sources 262 (2014) 112–122

Contents lists available at ScienceDirect

Journal of Power Sources

journal homepage: www.elsevier.com/locate/jpowsour

Manufacturing of industry-relevant silicon negative composite electrodes for lithium ion-cells

B.P.N. Nguyen [a], S. Chazelle [b,c], M. Cerbelaud [a,c], W. Porcher [b,c], B. Lestriez [a,c,*]

[a] Institut des Matériaux Jean Rouxel (IMN), Université de Nantes, CNRS UMR 6502, F-44322 Nantes Cedex 3, France
[b] CEA/LITEN, Grenoble, France
[c] Réseau sur le Stockage Electrochimique de l'Energie (RS2E), FR CNRS 3459, France

HIGHLIGHTS

- PAMA dispersant improves the stability of electrodes slurries of Silicon based negative electrode.
- Amount of PAMA must be limited due to competition in adsorption with CMC at the surface of CB particles.
- SBR copolymer latex improves adhesion of the tape to the current collector and increases cycle life.
- Calendaring is detrimental to electrochemical properties.

ARTICLE INFO

Article history:
Received 15 January 2014
Received in revised form
6 March 2014
Accepted 24 March 2014
Available online 2 April 2014

Keywords:
Lithium-ion battery
Silicon
Electrode formulation
Dispersant
Latex

ABSTRACT

In this paper, Poly (acrylic-co-maleic) acid (PAMA) is used as a dispersant to improve the stability of electrodes slurries for large scale processing of Silicon based negative composite electrode. The stability and homogeneity of the slurries are characterized using different techniques. Sedimentation test, electrical measurement, SEM-EDX observations as well as rheological measurements show that a more homogeneous distribution of carbon black (CB) inside the stack of Si particles is reached with presence of PAMA. However, the amount of PAMA is limited due to the competition in the adsorption of PAMA and Carboxylmethyl cellulose (CMC) at the surface of the CB particles. Upon cycling with capacity limitation, the optimized electrode formulation at lab scale could achieve more than 400 cycles with surface capacity ~2.5–3.3 mAh cm^{-2}. At the pilot scale, the improvement of adhesion of the tape to the current collector by using Styrene-co-Butadiene rubber copolymer latex (SB) helps to maintain long cycle life while calendaring is detrimental to electrochemical properties.

1. Introduction

Nowadays, rechargeable lithium-ion battery is one of the most promising energy storage technologies to enable a various range of clean transportations (hybrid electric vehicles, electric vehicles, Plug-in Hybrid Electric Vehicles). To meet requirements of these automotive applications, it is necessary to find higher capacity electrode materials for Li-ion batteries. The current commercial lithium ion battery is based on the use of graphitic carbon anode which provides a low theoretical capacity of 372 mAh g^{-1} and energy density (779 mAh cm^{-3}) [1]. Compared with graphite, silicon is a favourable alternative candidate due to a high specific capacity (3572 mAh g^{-1}) and specific volumetric capacity (2081 mAh cm^{-3}) [2]. However, poor performance of Si electrodes (large capacity fading and low cyclability) is a major issue. This could be explained by two distinct reasons: (i) Silicon exhibits dramatic volume expansion and shrinkage during lithiation and delithiation, respectively. This volumetric variation results in mechanical breakdown of the composite electrode [3,4]. (ii) Formation of unstable solid electrolyte interphase (SEI) causes uninterrupted liquid electrolyte degradation at the surface of silicon [5–7].

Several strategies have been undertaken to overcome these problems. One way is optimising the binder in order to cope at the molecular scale with the expansion and contraction of Si upon alloying and dealloying with Li. Most studies of Si anodes have involved the use of carboxymethylcellulose (CMC) and polyvinylidene fluoride (PVDF) binders. The most conventional binder PVDF used for the batteries is likely attached to Si particles via weak

* Corresponding author. Institut des Matériaux Jean Rouxel (IMN), Université de Nantes, CNRS UMR 6502, F-44322 Nantes Cedex 3, France.
E-mail address: bernard.lestriez@cnrs-imn.fr (B. Lestriez).

http://dx.doi.org/10.1016/j.jpowsour.2014.03.119
0378-7753/

Van der Waals forces only (between its fluorine atoms and hydrogen atoms). Moreover, PVdF is significantly plasticized by the liquid electrolyte solvents (carbonates) and becomes an easily deformable material with small resistance to deformations [8]. PVdF thus fails to accommodate large changes in spacing between the particles during battery cycling and quickly becomes incompetent in keeping the particles together and maintaining electrical conductivity within the anode, which is required for battery operation. In the meantime, noteworthy amounts of improvement have been achieved for CMC binders, which typically display a better performance and can be considered to be the state of the art in this field. CMC favours both (i) a much more homogeneous distribution of the carbon black conductive additive particles, (ii) an efficient networking process of the carbon black and Si particles in the composite electrode slurry, due to its extended conformation in solution that enables the formation of bridges between particles, and (iii) the establishment of a covalent bond through the esterification of the SiOH surface groups by the COOH functional groups of CMC, which increases the cycle life [9,10]. Since early works on CMC, [11–14] several other works proposed alternative binders to CMC, most of them being polysaccharides and/or bearing COOH functional groups [15–18].

Another way to improve the cycle life is using electrolytes containing a film-forming agent. In the case of silicon, unstable layer is formed in the first cycles without utilising FEC/VC additives and cracks occur on this layer during volume expansion upon Li insertion of the particles which exposes new surfaces leading to additional liquid electrolyte degradation [19–25]. Flexible polycarbonates form in the surface film in FEC and VC-containing solutions, which allows a better ability to accommodate the volume variations of the Si phase, then limiting the contact between the silicon particles and the liquid electrolyte [26]. This results in reduction of the amount of SEI products precipitating and accumulating inside the electrode at each cycle [25].

Besides, electro-conductive additives also display an important influence for the performance of Si-based electrodes. Combining carbon nanotubes (multiwall carbon nanotubes (MWNTs)) and nanofibers (vapor-grown carbon nanofibers (VGCFs)) allows building a hierarchical and resilient 3D conductive network, which strongly improves the cyclability of micron-size Si in Si/C/CMC composite electrodes [27]. In the case of nano-size Si, no improvement was found by using these carbon additives when compared to the standard carbon black (CB). However, by using reduced graphene oxide (rGO) instead of CB as the conductive additive for nano silicon based negative composite electrodes, a significant improvement of the electrochemical performance was confirmed, whatever the cycling conditions [28,29].

In this work, we aim to design the formulation of nanosilicon-based negative composite electrodes to wind some cylindrical cells. To reach this goal we looked for: (i) homogeneous and stable slurry-state, (ii) suitable mechanical properties for calendaring and battery assembly steps, (iii) long cycle life, for high active mass loadings of about 2.5–3.3 mAh per cm^2.

2. Experimental

Electrode preparation – Composite electrodes were made of nanometric Si (particle size 150 nm, specific surface area 14 $m^2\ g^{-1}$) as an active material (AM), Super P carbon black (CB, Timcal) as a conductive additive (C), Carboxylmethyl cellulose (CMC, DS = 0.9, M_w = 700.000 g mol^{-1} Sigma–Aldrich) and a Styrene-co-Butadiene rubber copolymer latex (SB) as a binder (B) and Poly (acrylic-co-maleic) acid (PAMA M_w = 3000 g mol^{-1} Sigma–Aldrich) as a dispersant (D).

At the lab scale, powders were introduced in a silicon nitride vial according to the electrode formulations given in Table 1. Then, 1 mL of buffer pH 3 0.1 M solution prepared with KOH and citric acid was added to 200 mg of composite electrode material. The solid loading is thus 17 wt%. Three silicon nitride balls (9.5 mm diameter) served as mixing media. A Fritsch Pulverisette 7 mixer was used to mill the slurry at 500 rpm for 60 min. The slurry was tape cast onto a 25 μm thick copper foil and dried for 12 h at room temperature and then at 2 h at 100 °C under vacuum. Citric acid and its salt, which are not eliminated by this vacuum treatment, remain in the composite tape.

At the pilot scale, CMC was dissolved in the buffer pH 3 solution, prepared with KOH and citric acid at 0.1 M. PAMA was added before introducing the conductive additive and the AM. The suspension is then dispersed using a high speed stirrer for 30 min. At the end of the dispersion, the latex is added and the slurry shortly homogenised. The slurries were coated using a semi industrial machine, with a comma bar system and an oven of 1 m length onto a 10 μm thick copper foil at a speed of 0.2 m min^{-1}. The transit time in the oven is so around 5 min.

Sedimentation test – Small amount (30 mg) of each material (Si, CB) was dispersed in buffer solution pH 3 by using ultrasounds for 15 min. The dispersant quantity was adjusted in order that its concentration (mg mL^{-1}) is the same as for electrode preparation. The process of settling was observed visually as a function of time.

Rheological measurements – Rheological properties were measured on a controlled-stress rotating rheometer (Anton Paar,

Table 1
Composition, porosity, thickness and mean resistivity (measured with 2 probes) of composite electrodes. L and P mean an electrode prepared at the lab scale and at the pilot scale, respectively.

Electrode name	Si (wt%)	CB (wt%)	Latex (wt%)	CMC (wt%)	Buffer (wt%)	PAMA (wt%)	Porosity (%)	Thickness (μm)	Loading (mg Si cm^{-2})	Conductive additive volume fraction[a] (%)	2-probes resistivity with stand. dev. (ohm cm)
La	–	51	–	16	33	–	n.m.	n.m.	n.m.	n.m.	n.m.
Lb	–	49	–	15.7	31.8	3.5					
Lc	–	47	–	15.2	31	6.8					
Ld	–	43.2	–	14.4	29.5	12.9					
L1	67.6	10.1	–	6.8	15.5	–	71–73	66–68	2.6–2.8	3.06	11.6 ± 0.5
L2	65.9	10.1	–	6.8	15.5	1.7	68–70	63–65		3.30	7.6 ± 0.5
L3	64.2	10.1	–	6.8	15.5	3.4	65–68	60–62		3.55	12.7 ± 0.5
P1	65.9	10.1	–	6.8	15.5	1.7	70–71	52–54	2.0–2.1	3.24	11.4 ± 0.5
P2	63.5	9.7	3.6	6.6	15	1.6	68–69	50–51		3.14	9.5 ± 0.5
P3	61.3	9.4	6.9	6.3	14.5	1.6	68–69	52–54		3.01	11.1 ± 0.5
P1	65.9	10.1	–	6.8	15.5	1.7	59–60	41–42	2.0–2.1	4.40	9.4 ± 0.5
P2	63.5	9.7	3.6	6.6	15	1.6				3.97	8.1 ± 0.5
P3	61.3	9.4	6.9	6.3	14.5	1.6				3.85	9.7 ± 0.5

n.m. is for not measured.
[a] The volume fraction is calculated by taking into account the electrode porosity.

MCR 101) with a 50 mm diameter plane-and-plane geometry and the sample gap between the Pelletier plane and the geometry was fixed at 0.6 mm. Several types of rheological measurements were carried out: (i) Two measurements were done with continuous shear: a rate sweep measurement from 0.1 to 1000 s^{-1} to determine the viscosity of the slurries and sequence at constant rate measurement 10 s^{-1} for 900 s to simulate and follow what happens upon gentle mixing as in the reservoir of the slot die machine. (ii) The evolution of moduli at a frequency of 1 Hz and a strain of 1% after a preshear at 100 s^{-1} for 60 s to simulate and follow what occurs after casting.

Study of electrode's texture – Scanning electron microscopy (SEM) and Energy dispersive x-ray imaging was performed by using a JEOL JSM 7600 to investigate textural properties of composite electrodes.

Electrical measurements – Electronic resistivity measurements were carried out by impedance spectroscopy on dry Si electrode/current collector samples sandwiched in between two metallic plungers in a standard swagelok cell, using a VMP automatic cycling/data recording system (Biologic). The frequency range was scanned from 10 mHz to 189 kHz. Several compositions were studied at different thicknesses. Six samples were evaluated for each composition. The measure was repeated three times on each sample. The impedance diagrams were resumed in all cases to a single point on the real axis. A linear increase of the resistance, R, with the thickness, t, was found, with $R = 0$ for $t = 0$. The latter implies that the contact resistance between the copper foil used as current collector and the composite electrode is negligible in the dry state. The electrode resistivity, ρ, was thus determined from the well-known equation $\rho = (R \times S)/t$, where S is the contact surface area between the probe (metallic piston) and the sample, 0.283 cm^2.

In complement, a mapping of the electronic resistivity of dry Si composite tapes prepared on plastic film was also measured by using four-point probe mapping system (model 280SI-Microword) with computer controlled stepping motors to move the four-point probe. The spacing between each probe is 1 mm. Each probe has a contact area radius of 100 μm and the load applied on each probe is 60 g. The current source is a fixed-output, range-programmable constant-current generator, and provides an appropriate amount of test current to the sample under test. It is automatically selected by the measurement board during the measurement sequence.

Electrochemical testing – Half cells: two-electrode Swagelok™ test cells comprise (i) a 0.78 cm^2 disc of composite positive electrode (ii) a porous glass paper as separator soaked in an electrolyte consisting of 88 wt% LP30 [1 M $LiPF_6$ solution in dimethyl carbonate-ethylene carbonate (1:1)] 2 wt% vinylene carbonate and 10 wt% fluoroethylene carbonate mixture and (iii) a 0.78 cm^2 Li metal disc as the negative and reference electrode. The cells were assembled in the glove box under argon atmosphere. Cell cycling was performed at 20 °C, monitored by a VMP™ system (Biologic) in a galvanostatic mode. The voltage range used was 0.01–1 V versus Li^+/Li. All composite electrodes were studied with the same rate (C/5 and D/5) with a limited discharge capacity of 1200 mAh g^{-1}_Si (850 mAh g^{-1}_electrode).

3. Results

3.1. Elaboration at the lab scale: selection of a dispersant

Our previous works show that preparing the electrode in a pH 3 buffer is mandatory to achieve the grafting of the CMC binder which strongly improves the cycle life [30]. However, at pH 3, the zeta potential of the Si particles is equal to zero and the slurries are not stable and flocculate through the attractive Van der Waals interactions [31]. Thus we looked for a dispersant to improve the stability of the electrode slurries for large scale processing. In the aqueous-processing of $LiFePO_4$, poly(4-styrene sulfonic acid) (PSSA), poly(acrylic acid-co-maleic acid) (PAMA), polyethyleneimine (PEI) and the isooctylphenylether of polyoxyethylene (Triton X-100) were considered as highly efficient dispersants to have good dispersion property [32–35]. While in non-aqueous processing, the study of C–C. Chang et al. demonstrated improvement of $LiFePO_4$ and KB electrode by using polyacrylate based dispersant [36]. In aqueous-processing of $LiCoO_2$, it's found that both $LiCoO_2$ and carbon powders can be well-dispersed by using ammonium polyacrylic acid (PAA-NH_4), resulting in a decrease of powder aggregation and an increase in the contact area between $LiCoO_2$ and the conductive additives [37,38]. In addition, J.T. Patey el al. proved the role of Triton X-100 in improvement of distribution of the suspensions of TiO_2 and CB, leading to improved electrical contact between particles [39]. With respect to the use of dispersants, no study concerned Si-based negative composite electrodes. Here, different dispersant were tried and we will report the results achieved with PAMA.

In order to identify the dispersing efficiency of PAMA on Si and CB, dilute suspensions in pH 3 buffer were prepared and their dispersion stabilities were observed by sedimentation tests. Fig. 1 shows different buffer suspensions of Si, CB, mixture of Si + CB in the presence of PAMA (with identical concentration in mg L^{-1} as in the electrode slurry of L2) and without PAMA, respectively, after different time periods. In the initial state, Si, CB and mixture of them were homogeneously distributed in the suspension with addition of PAMA, while without PAMA the CB powder began to settle especially in the suspension of both Si + CB with the

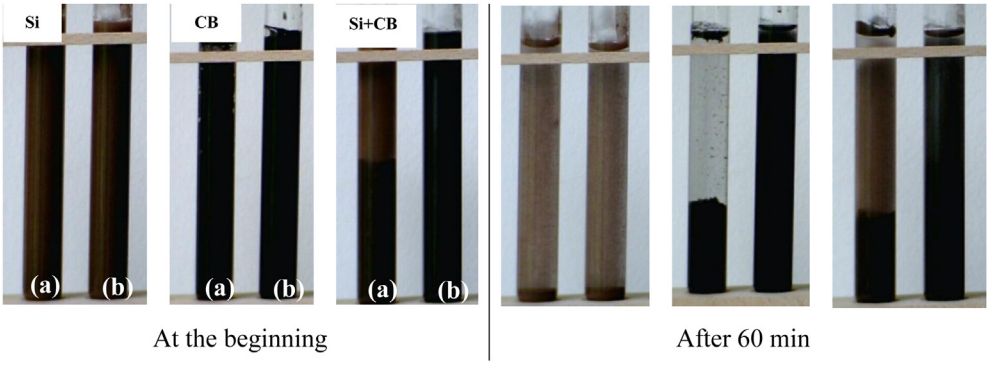

Fig. 1. Settling test of different suspensions (Si, CB, Si + CB in pH3 buffer) as a function of time: (a) without PAMA, (b) with 4 mg mL^{-1} of PAMA (which is the same concentration as in the slurry of electrode L2).

segregation into two separate phases (CB at the bottom and Si in the upper supernatant). After 1 h, most of Si or CB powder settled to the bottom in the suspension without PAMA and only small amount of Si powder was suspended in the upper supernatant. In contrast, the phenomena were apparently different in the suspension with PAMA. CB powder was still homogeneously distributed and mixture of Si + CB remained stable, although Si without CB settled to the bottom of the vial. From the above sedimentation results, it clearly indicates that PAMA doesn't provide better stability of Si in buffer solution while an improvement of stability of CB was displayed practically. Regarding the suspension of both Si + CB, PAMA remains an efficient dispersant as the settling phenomenon is very much decreased.

Complementary visual observations of CB/CMC/PAMA/buffer composites (without Si) are shown in Fig. 2. To prepare these blends we kept the same ratio of the mass of PAMA vs. the powder surface area (Si + CB) as in composite electrodes. One can observe in Fig. 2 that with increasing PAMA content, a demixing occurs between CB (dark zones) and one of the two polymers, CMC or PAMA. Such a demixing between a powder and a polymer generally occurs when a polymer does not adsorb at the surface of the particles. Non adsorbed polymers are excluded from the particle surfaces and the particles may flocculate by the mechanism of depletion [40–42]. The settling tests clearly shows a stabilization of the CB suspensions by PAMA which must results from the adsorption of PAMA and the establishment of repulsive electrostatic forces between the CB particles. The adsorption of PAMA on carbon surface has been shown elsewhere [33]. On another hand, CMC is also known to show attractive interactions with carbon surfaces and generally strongly adsorbs on it [43–45]. It is well known that when more than one polymer is present in a suspension, some competitive absorption can occur between the different polymers [46]. Thus, we may hypothesize that by increasing the PAMA concentration in the CB/CMC/PAMA/buffer mixtures (Fig. 2) the competition between CMC and PAMA resulted in the exclusion of the CMC from the CB particle surfaces. Whatever it is, a competition between CMC and PAMA with respect to adsorption on CB is evidenced. Same kind of visual observations show however no difference between L1 (0), L2 (1.7) and L3 (3.4 wt% PAMA) composite electrodes. L2 tape is shown in Fig. 3. It can be noted some detachments from the copper current collector, as for most of the lab-made tapes studied here.

Further SEM observations exhibit the morphology of composite electrodes with and without PAMA. After ball milling, all particles are fairly well dispersed at micro scale (Fig. 4(a)–(c)). The electrodes prepared with PAMA show visually a higher compactness (and a lower porosity, Table 1), which is another evidence of the better stability of their slurries. Larger agglomerates are formed in

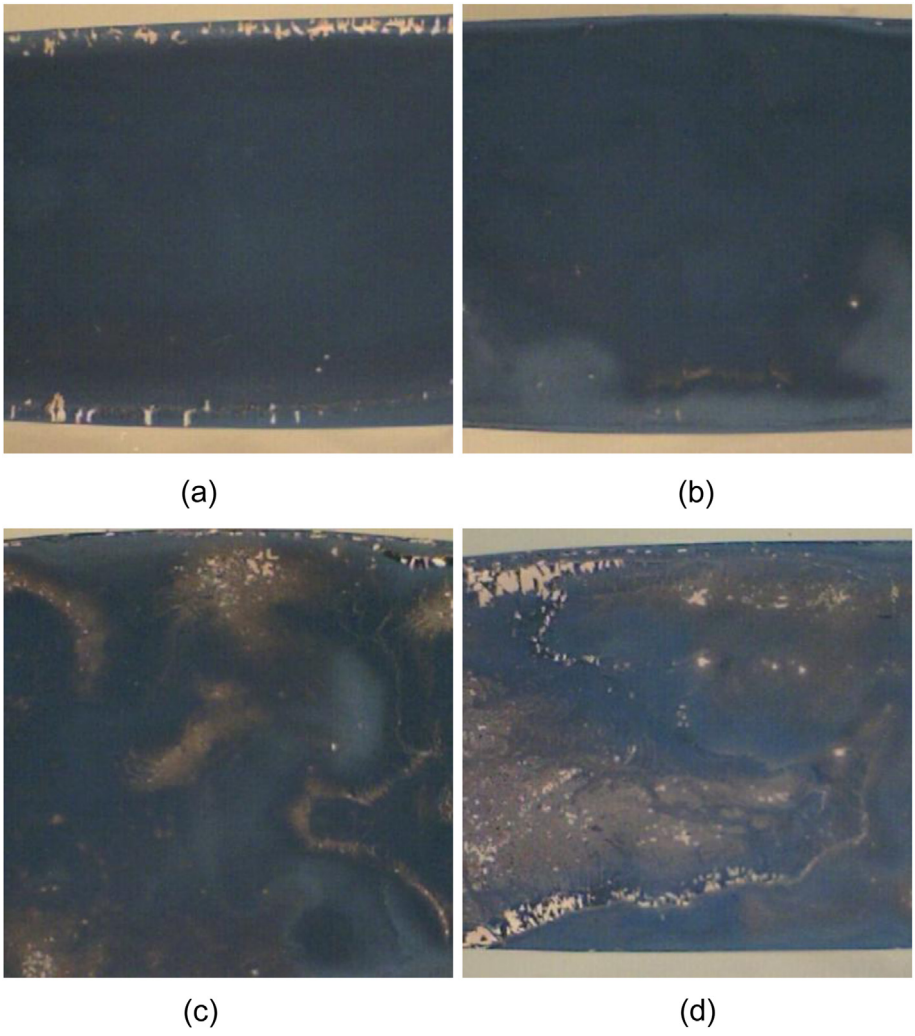

Fig. 2. Camera pictures of CB/CMC/PAMA/Buffer tapes with varying amounts of PAMA: (a) La, (b) Lb, (c) Lc and (d) Ld tapes.

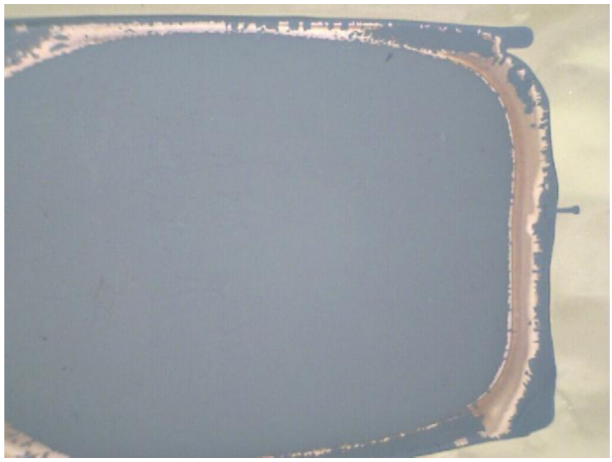

Fig. 3. Camera pictures of L2 tape.

less stable slurry which results in a higher porosity. EDX measurements at high magnification were utilized in order to more finely characterize the distribution of CB and Si in the electrodes. It can be seen from Fig. 4(d)–(i) that the dispersion within the composite electrodes seems to be better with presence of PAMA with less area which has rich carbon than without PAMA.

In order to verify the role of PAMA in dispersion of CB particles within the dried composite electrodes, two types of electrical measurements were carried out (Fig. 5(a)). Fig. 5(b) shows the resistance, R, of L2 electrode/current collector samples sandwiched in between two metallic pistons as a function of the Si electrode thickness, t. One can observe a linear increase of R with t, with $R = 0$ for $t = 0$. The latter implies that the contact resistance between the copper foil used as current collector and the composite electrode is negligible in the dry state. Average values of the electrode resistivity with different PAMA compositions are given in Table 1. There is variation of the resistivity with the amount of PAMA. It starts decreasing when PAMA is used and reaches the minimum at 1.7 wt% for L2 then increases for L3. It confirms that PAMA could help in the dispersion of the conductive additive leading to a decrease of resistivity by nearly a factor of 2. However, at high amount of PAMA (3.4wt%), it contributes to the increase of the resistivity as it also increases the electrically insulating organic matter content [37,38]. In complement, Fig. 5(c) shows resistivity scans on the different composite tapes L1-L2 using four-probes measurement technique on samples that were tape cast on plastic film. The results are displayed as values of resistivity (in ohm square) along lines at different positions as schematized in the drawing of Fig. 5(a). Without addition of PAMA, the spatial distribution of sheet resistance in L1 is large and mean value of resistivity is higher than for others. One can see that the presence of PAMA in L2 helps to lower the distribution in resistivity through the sheet, likely due to improved CB powder dispersion. In fact a fairly homogeneous value of resistivity is observed. We believe that the spatial distribution of sheet resistance in L1 reflects the size of variations in the homogeneity of this electrode.

Finally, cycling tests were done in order to evaluate the electrochemical behaviour of the different electrodes. As can be observed from Fig. 6(a), the battery cycle life strongly depends on the amount of PAMA in the composite electrode. Without using PAMA (L1), the batteries can achieve around 200 cycles while with 1.7 wt% of PAMA (L2), the cycle life increases more than 2 times (415 cycles). However, when 3.4 wt% PAMA (L3) is used, the cycle life decreases sharply (30 cycles). Coulombic efficiencies over the first

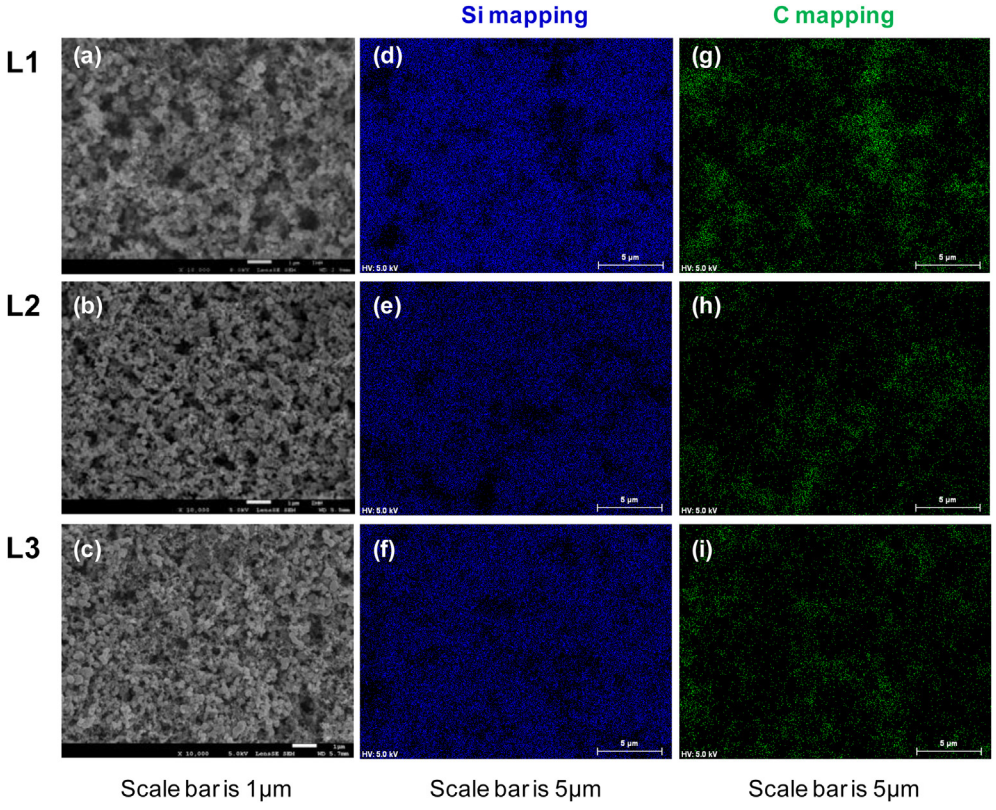

Fig. 4. (a–c) SEM observations and (d–i) EDX mappings (Si and C) of (from top to bottom) L1, L2 and L3 electrodes.

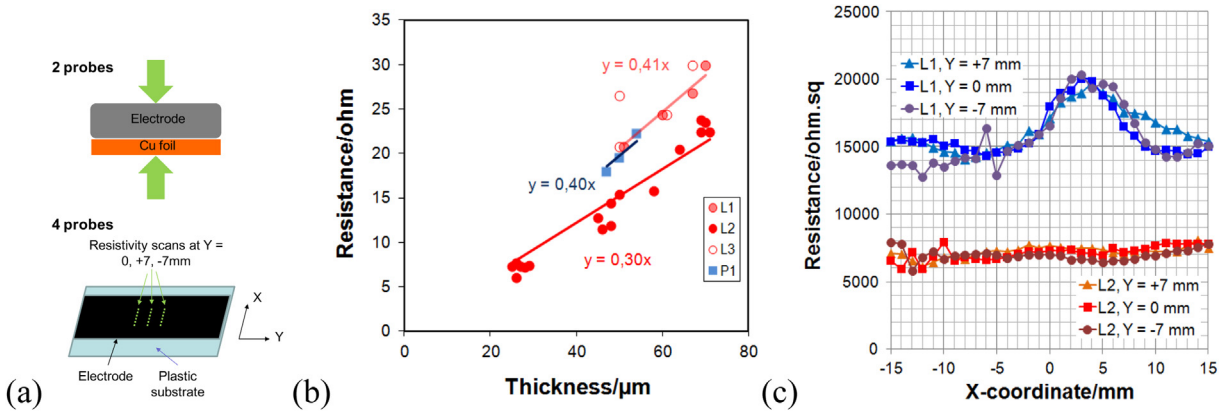

Fig. 5. (a) Schematic drawings of the 2-probes and 4-probes electrical resistance set-up. (b) Resistance of dry electrode/current collector samples sandwiched in between two metallic pistons as a function of the electrode thickness (2-probes). (c) Variation in the resistivity through the tape width (over 3 cm) at different position along the tape (at +7 and −7 mm above and behind a central line) (4-probes).

50 cycles are 99.1, 99.3 and 91.4% for 0, 1.7 and 3.4 wt% PAMA, respectively. The incremental capacity curves are shown in Fig. 6(b)–(d) for L1 to L3. Let's remind that electroactivity of Si is characterized by two major steps, A and B, which have been ascribed to Li reactions with amorphous Si [47]. Li_xSi alloys formed in step B are lithium rich compared to step A. The capacity which corresponds to step A is ca 1875 mAh g^{-1}. Thus, when cycling is done with a capacity limitation of 1200 mAh g^{-1}, only step A must be involved if all the Si particles are active, i.e. are electrically wired to the current collector. The curves at the 2nd cycle show that initially there is an activation step of the electrode as the capacity is sought from both steps A and B. However, after 100 cycles one can see only step A in the incremental capacity curves for L1 and L2. With higher number of cycles, for example 160, one can see the appearance of step B in L1 which shows that the number of Si particles which remain electrically wired has decreased and that

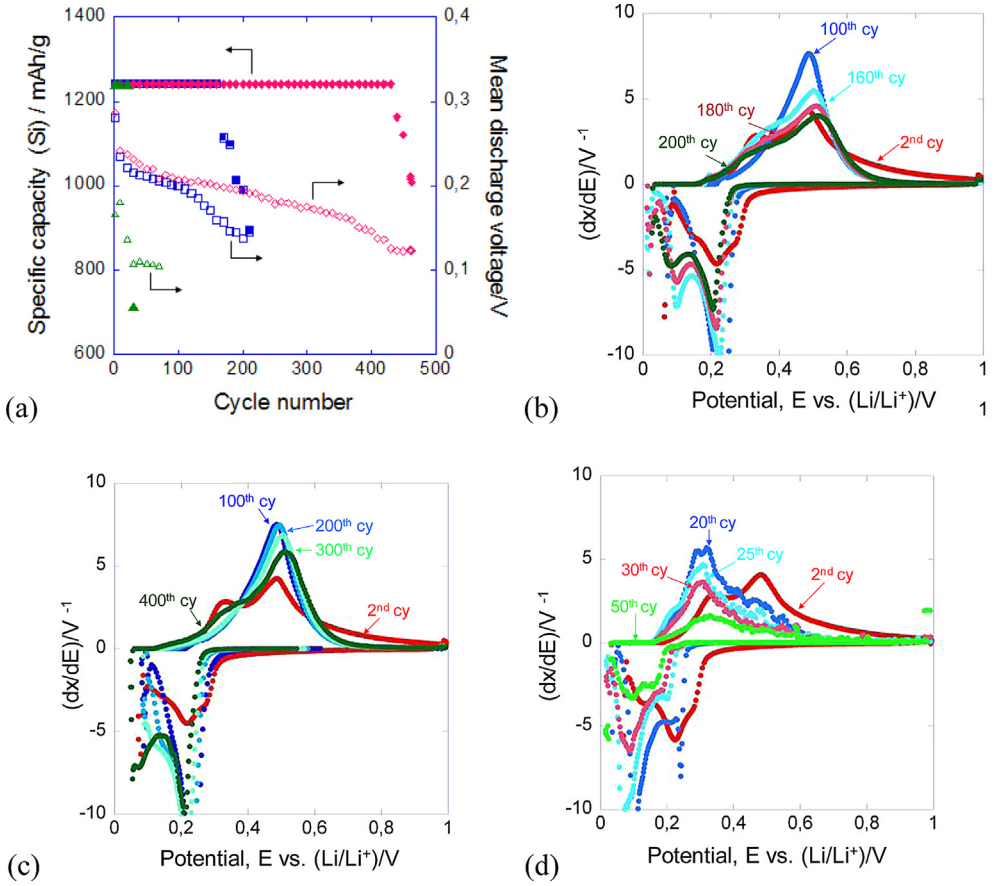

Fig. 6. (a) Discharge capacity (■, ◆, ▲) and mean discharge voltage (□, ◇, △) versus number of cycle for electrode formulations with capacity limitation of 1200 mAh per g of Si and different amount of PAMA: (■, □) 0 (L1), (◆, ◇) 1.7 (L2) and (▲, △) 3.4 wt% PAMA (L3). The Si mass loading is 2.6 mg cm^{-2}. Incremental capacity curves at selected cycles for electrode formulations with different amounts of PAMA: L1 (b), L2 (c) and L3 (d).

Table 2
Mass and thickness of electrodes, mass of Si, mass gained Δm and thickness variation, cumulative capacity loss after cycling, number of electrons n (e_{lost}), average weight M_{srp} of side reaction products.

$m_{electrode}$ (mg)	m_{Si} (mg)	Thickness (μm)	Mass gained Δm (mg)	Thickness variation (μm)	Cummulative Capa. loss (mAh/g)	n(e_{lost}) (mol)	M_{srp} (g mol^{-1} e^- loss)
3.45	2.28	65	6.40	56 ± 3	1472	$1{,}24.10^{-4}$	51
3.45	2.28	65	6.91	58 ± 3	1696	$1{,}44.10^{-4}$	48

only a fraction of the total Si mass remains electrochemically active. Contrarily, for L2 with 1.7 wt% PAMA and up to 300 cycles, only step A is involved for delivering the 1200 mAh g^{-1} capacity, which shows that a much larger Si mass remains electrochemically active in L2 compared to L1. In the case of L3, the incremental capacity curves show that the capacity is sought from a minor part of the Si active mass as both steps A and B are involved all along the short cycle life.

Here, as already observed, [25] there is a relationship between the cycle life and the coulombic efficiency. When silicon is cycled with capacity limitations, the first cause of fading is the liquid electrolyte degradation rather than the mechanical disintegration if the electrode is properly formulated [25,48,49]. Higher the coulombic efficiency, then lower the liquid electrolyte degradation, and thus longer the cycle life is. We note that as in previous work [25] a post-mortem analysis reveal a thickness increase and a mass-uptake of the composite electrodes. The weight and thickness variations of different electrodes L2 were followed (ex-situ measurements) after 100 cycles and correlated to the cumulative irreversible capacity loss which is defined as the sum over all cycles of the excess discharge versus charge capacity at each cycle (Table 2). The results are in agreement with D. Mazouzi's work. They highlight the occurrence of the liquid electrolyte degradation which products precipitate within the electrode porosity. One can see that improving the CB distribution with PAMA (from L1 to L2) slightly improves the coulombic efficiency and significantly improves the cycle life. We believe this better stability upon cycling (more uniform functioning of the Si active mass) is due to a more uniform mechanical stress distribution and more uniform electronic conductivity within the composite electrode as a consequence of the more uniform carbon black distribution [29]. L3 has dramatically short cycle life and very poor coulombic efficiency. The SEM-EDX pictures show a rather homogeneous distribution of the CB particles within the composite electrode and the electrical properties of the pristine L3 electrode are at the level of L1. A plausible interpretation is a lack of mechanical strength in this composite electrode as a consequence of the competition between PAMA and CMC which would result in less CMC bridging [14] between the different particles when the PAMA content increases. Another interpretation could be a parasitic reaction between the PAMA additive and the liquid electrolyte. This hypothesis was checked by cyclic voltammetry in the 0.05–2.5 V range at the rate of 1 and 5 mV s^{-1} on the CB/CMC/PAMA/Buffer tapes of Fig. 2. Whatever the PAMA content (from 0 to 12.9 wt%) the

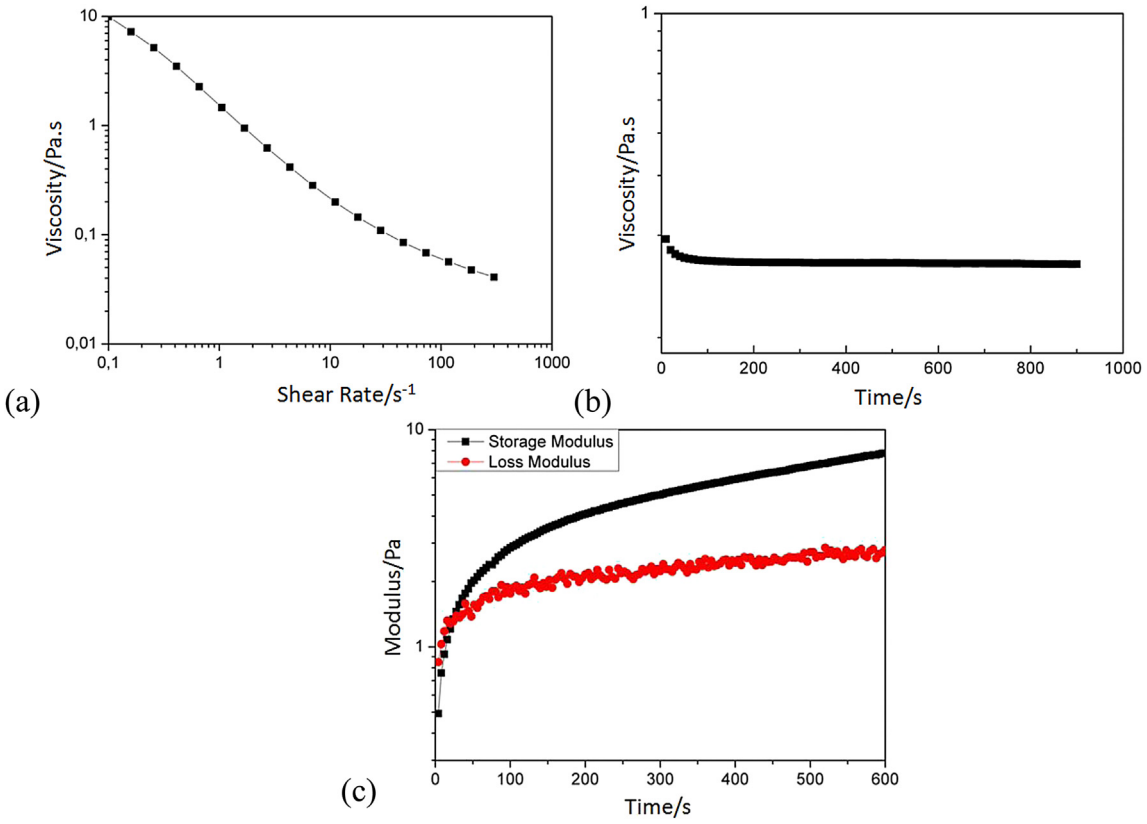

Fig. 7. Rheological properties of L2 slurry: (a) The evolution of viscosity as a function of shear rate. (b) The evolution viscosity as a function of time at a shear rate 10 s^{-1}. (c) The storage modulus and loss modulus as a function of time at a frequency of 1 Hz and a strain of 1% after pre-shear at 100 s^{-1} for 60 s.

voltammograms are similar and do not evolve upon cycling (not shown). Thus we may conclude that there is no parasitic reaction associated with the presence of PAMA.

In summary, the results obtained by sedimentation test, electrical measurements and SEM-EDX observations show that a more homogeneous distribution of CB inside the stack of Si particles is reached with PAMA. Two scales of heterogeneity are disclosed when no dispersant is added. At the microscale (EDX observations on 500 μm^2) larger CB clusters of about 5 μm diameter are detected while at the macroscale (resistivity mapping on 9 cm^2) zones of about 1 cm diameter with much higher (33% higher) resistivity are observed. As a consequence of the more uniform CB dispersion, a much better electrochemical behaviour is displayed with significantly improved coulombic efficiency and cycle life. However, if PAMA is added in too large concentration (3.4 wt% here), a very poor coulombic efficiency and cycle life are observed, which could be attributed to the competition in the adsorption of PAMA and CMC at the surface of the particles. The adsorption of PAMA to the CB surface likely impedes the adsorption of the CMC chains and thus the formation of bridges between the CB particles and the Si mass which results in a catastrophic failure upon cycling. As a conclusion of this part, the electrode formulation L2 was selected for being processed at the pilot scale.

Before the transfer from the lab to the pilot scale, the rheological properties of L2 slurry were checked. The viscosity vs. shear rate is given in Fig. 7. A shear-thinning behaviour is observed (i.e., a decrease of the viscosity with increasing shear rate). Fig. 7(b) display viscosity versus time at constant shear rate. There is a small decrease of the viscosity at the beginning; nevertheless the plateau seen after 60 s depicts the stability of slurry upon gentling mixing as in the reservoir of coating machine. In order to model the process after coating, the electrode slurry was preliminary sheared at 100 s^{-1} for 60 s. Then the evolution of the storage G′ and loss modulus G″ vs time was recorded [50]. Under very small strain

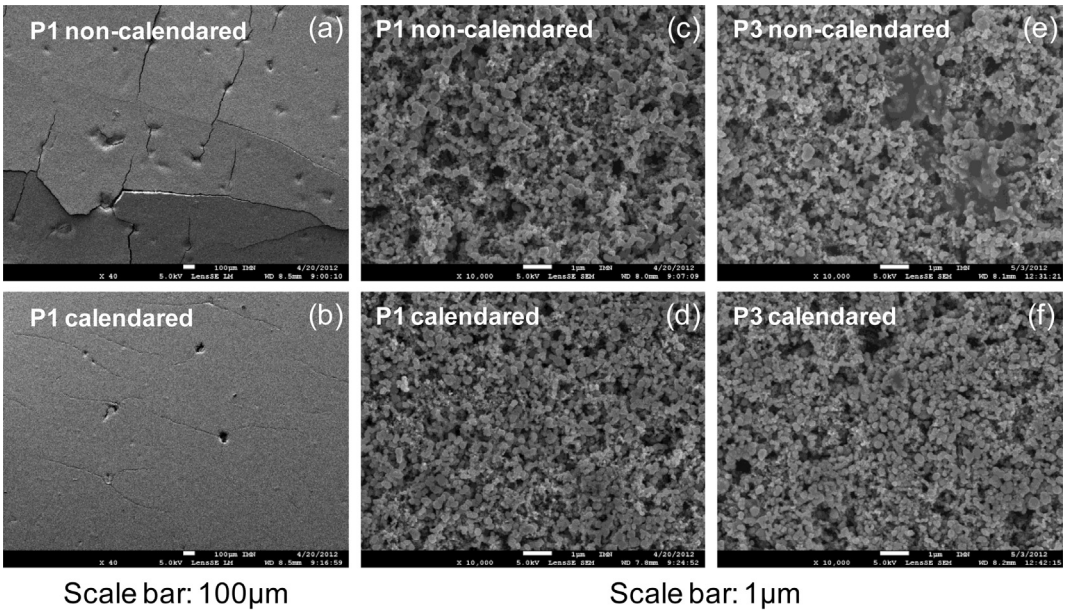

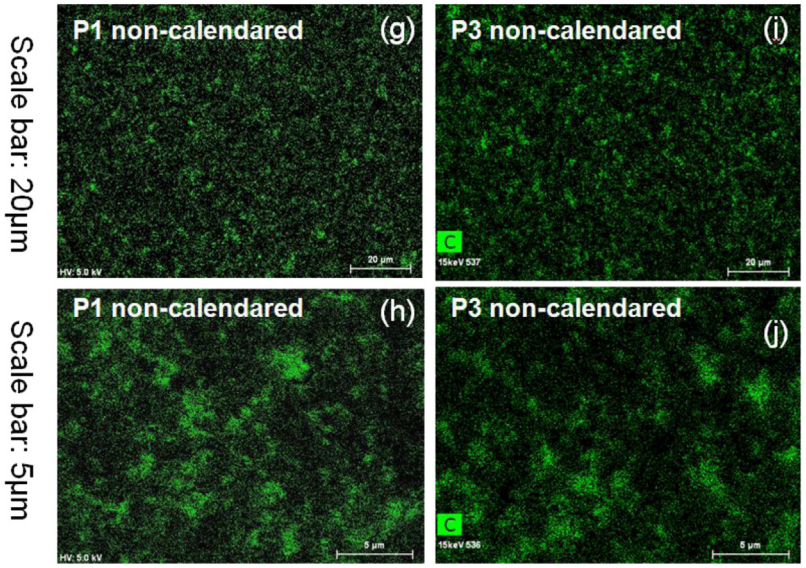

Fig. 8. SEM images for electrode P1 (a,c) uncalendared and (b,d) calendared down to 60% porosity; electrode P3 (e) uncalendared and (f) calendared down to 60% porosity. The EDX mapping image for Carbon at two different magnifications in P1 (g, h) and in P3 (i,j).

amplitude applied, the variation with time of the moduli reflects the spontaneous rearrangements or relaxations into the slurry at rest. As can be seen from Fig. 7(c) a solid like behaviour is rapidly reached and G′ dominates G″ after 60 s. This means that after short time, settling is virtually stopped by the mechanical percolation throughout the sample of the solid network of particles. After shear the moduli keep increasing upon time as a function of internal reorganization within the slurry. According to these measurements, the rheological properties of the slurry with PAMA dispersant are then suitable with the pilot line requirements.

3.2. Elaboration at the pilot scale: addition of an elastomeric latex binder and calendaring

The slurry was prepared with a total amount of 350 g and a solid loading of 21%. Its rheological properties were also characterized to validate that they were in the process window of the coating machine. Results (not shown) give a viscosity between 1 and 10 Pa s for shear rate of 1–100 s^{-1} in the range of the coating machine. There is a factor 10 between the viscosity of the slurry prepared in the lab and the one prepared at the pilot scale, a consequence of the higher solid loading of the latter compared to the former, i.e. 21 vs. 17 wt%. The slurry is observed to be stable at rest, with G′ which is superior to G″ in the low frequency range. These data show that the rheological properties of the slurry are well adapted to a coating process with a comma bar system.

However, the tape obtained after coating this slurry showed a low adhesion to the copper current collector (Fig. 8(a)). Moreover, the suppleness was not enough for winding the electrode. Two complementary strategies to improve this adhesion were evaluated: the addition of a complementary elastomeric binder (a styrene-co-butadiene rubber copolymer in the form of a latex) and the calendaring of the electrode (Fig. 8(b)). Indeed, it is known that to improve the adhesion to the current collectors of aqueous processed electrodes, mixture of CMC and emulsion polymerized styrene-butadiene copolymer latex (SB) could be used [11,12,51–53]. SB is a flexible polymer with large breakage elongation, which improves the mechanical stability of the electrode. Interestingly, a latex does not perturb the rheological properties of the slurry. It was added in the end of the mixing step to avoid any competitive adsorption with CMC [54].

Adhesion was evaluated qualitatively, using a scotch and making a peeling test manually; the suppleness was estimated by winding electrodes around mandrels of different diameters. Results are grouped in Table 3. If the electrode is not calendared, then the suppleness is fairly low. Cracking and eventually debonding of the electrode is seen when one try to wind it around a mandrel of 30 mm or less diameter. The calendaring step allows enhancing significantly the electrode suppleness. In complement, adding SB (in P2 and P3) allows to completely fold the electrode and to handle it.

Table 3
Adhesion and suppleness (min diameter at which the electrode can be wound before cracking and detaching from the current collector) of the electrode following the latex proportion (P2: 3.6 wt% and P3: 6.9 wt%) and the electrode porosity.

Electrode name	Porosity (%)	Adhesion	Suppleness (mm)
P1	70	Bad	>30
P2		Good	>30
P3		Good	>30
P1	65	Bad	10
P2		Good	2
P3		Good	0
P1	60	Bad	5
P2		Good	0
P3		Good	0

The morphology of the tape cast electrodes were observed by SEM (Fig. 8(c–f)). The images suggest a similar morphology than the electrodes prepared at the lab scale. Rather good homogeneous distribution of Si and CB were observed with P1 and P2. Nevertheless, at the highest SB content (P3), it could be observed some rich SB zones (Fig. 8(e)), a possible consequence of SB migration during the drying step [55,56]. With and without calendaring step, the dispersion of all particles in composite tape is identical. Calendaring reduces the porosity (Compare Fig. 8(c),(e) to (d),(f)). As can be seen from SEM-EDX chemical mapping (Fig. 8(g–j)), the CB appears less well distributed than in the composite electrodes prepared in the lab (Fig. 4) which could be ascribed to the different processing scales involved. Indeed, the preparation of electrodes at the lab scale implies small quantities and short mixing and casting durations, while at the pilot scale much larger quantities and much longer mixing and casting durations are implied. In particular, it is known that longer duration is detrimental to the stability of a slurry and thus to its homogeneity. The comparison of the electrical measurements in Fig. 5(b) and in Table 1 agrees with a poorer distribution of the CB as the electrical resistivity of P1–P3 are higher than L2, i.e. 9.5–11.4 vs. 7.6 Ω.cm for non-calendared P1–P3 vs. L2, respectively. Calendaring decreases the electrical resistivity to 8.1–9.7 Ω.cm for calendared P1–P3.

Finally, to evaluate the electrochemical behaviour of the electrodes prepared at the pilot scale, cycling tests were done at capacity limitation of 1200 mAh per g of Si. The same behaviour was observed as for L1-L2 in all cases, i.e. a first activation period where the mean discharge voltage is seen to increase and then a steady decrease of the latter (Fig. 9(a)). At some point of the battery life, the mean discharge voltage shows a faster decrease which is preceding the end of life. In fact, the capacity is observed to drop from the 1200 mAh per g when steps B starts to be involved as seen on the incremental capacity curves (Fig. 9(b–d)). Thus, we may conclude that the same degradation mechanism operates than in L1-L2. The slow mechanical disintegration of the composite electrode and the continuous precipitation of liquid electrolyte degradation products within the composite electrode porosity progressively disconnect the active particles. When one compares the different electrodes, a longer cycle life is mirrored in a slower polarization drop in mean discharge voltage.

The P1 electrode which is non-calendared and contains no latex as L2 shows a lower cycle life than the latter, i.e. 100 vs. 450 cycles, a result which could be attributed to a poorer CB distribution in P1 vs. L2 and a lower adhesion of P1 to the Cu copper collector than L2. The cycle life is compared for P1, P2 and P3 for their different porosities in Fig. 10(a). Without calendaring and at high porosity (~69%), the cycle life increases with increasing the amount of latex, i.e. with increased adhesion. In other work it was shown that the improvement of the adhesion by roughening of the copper current collector was strongly increasing the cycle life by decreasing the rate of active mass disconnection [57]. A possible interpretation is that the electrode, being swollen by the liquid electrolyte degradation products, an internal stress grows which results in the detaching of parts of the electrode from the current collector. A higher adhesion keeps the electrode attached and electronically wired to the current collector for a higher number of cycles. Another general trend is a shorter cycle life when the porosity is decreased (when the electrode is calendared). Several causes may individually or altogether explain this result. A lower porosity implies more mechanical constraints within the composite electrode upon alloying of the Si particles [58]. Moreover, a lower porosity means less volume to accommodate the precipitation of the liquid electrolyte degradation products. Furthermore, the calendaring step could damage the CMC bridges between the Si and CB particles, decreasing the mechanical strength at this molecular level.

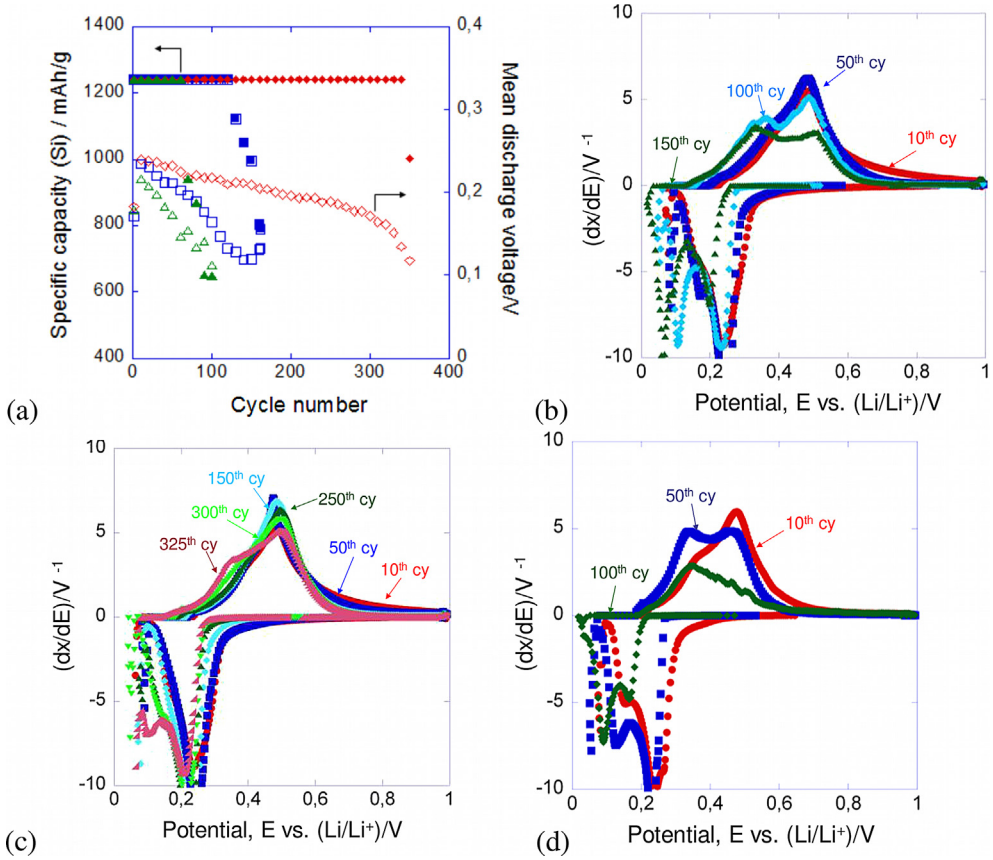

Fig. 9. (a) Discharge capacity (■, ◆, ▲) and mean discharge voltage (□, ◇, △) versus number of cycle for electrode formulations with capacity limitation of 1200 mAh per g of Si and different latex content or porosity: (■, □) P1 without calendaring, (◆, ◇) P3 without calendaring, and (▲, △) P3 with calendaring down to 60% porosity. The Si mass loading is 2.0–2.1 mg cm^{-2}. (b) Incremental capacity curves at selected cycles for (b) P1 without calendaring, (c) P3 without calendaring, and (d) P3 with calendaring down to 60% porosity.

This way, an interesting feature is observed in Fig. 10(b). One can see that the maximum mean discharge potential (reached at the end of the electrode activation step) shows a clear decrease with a decrease in porosity. The mean discharge voltage is influenced by both the (i) electrode resistance and the (ii) fraction of active mass that is electrochemically active. A lower mean discharge voltage means either or both (i) more resistive electronic and/or ionic wiring of the active mass; (ii) a lower fraction of active mass that is electrochemically active, with in the case of Si cycled with capacity limitations, a deeper extent of lithiation of the active mass to deliver the capacity, and as a consequence a lower discharge voltage. Thus the results in Fig. 10(b) confirm that calendaring has a detrimental effect of the composite electrode architecture efficiency with respect to its electrochemical behaviour.

A disappointing conclusion from the applied point of view is that to achieve long cycle life, Si-based composite electrodes must be highly porous (or the Si volume fraction must be kept low [58]) which results in low volumetric capacity. We can calculate for

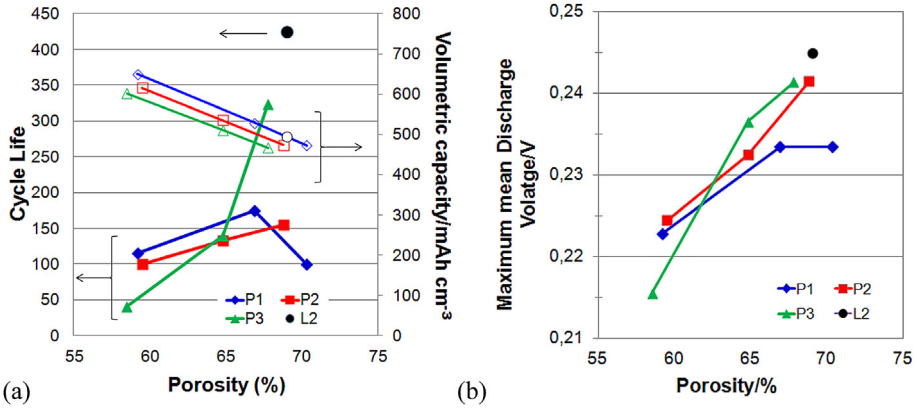

Fig. 10. (a) Cycle life and the calculated volumetric capacity of the electrodes for L2, P1, P2 and P3 as a function of the porosity. (b) Maximum value taken by the mean discharge voltage for L2, P1, P2 and P3 as a function of the porosity.

typical graphite-based electrodes with 30% porosity and 80 wt% graphite in the dried electrode composition (which gives a volume fraction of 60% for graphite), by considering a specific capacity of 350 mAh g^{-1}, that the volumetric capacity is 475 mAh per cm^3 of composite electrode. Here, higher values are achieved only if the Si-based composite electrodes are calendared down to 65% and less. However in such a case the cycle life of electrodes prepared at the pilot scale is decreased down to 150 cycles.

4. Conclusion

We have successfully designed the formulation of nano-silicon based negative composite electrodes with homogeneous morphology which could operate more than 400 cycles at 1200 mAh g^{-1} of Si limitation and a surface capacity is ~3.3 mAh cm^{-2} when prepared at the lab scale. In addition, the role of the PAMA dispersant has been investigated. This one could help not only to achieve high homogeneity of the electrode, especially uniform carbon black distribution prepared at the lab scale which leads to improvement of cyclability and coulombic efficiency in half cell, but also facilitate the powder incorporation at the pilot scale. However, the amount of PAMA was optimized at 1.7 wt% because a competitive adsorption occurs between PAMA and CMC versus the CB particles. At too high content (3.4 wt%) the adsorption of PAMA to the CB surface impedes the adsorption of the CMC chains and thus the formation of bridges between the CB particles and the Si mass which results in a catastrophic failure upon cycling. At the pilot scale, in order to wind cylindrical cells, the adhesion of the tape to the copper current collector needs to be improved by calendaring and adding the latex SB. Our electrochemical study of different electrode formulations prepared at pilot scale indicates that to achieve long cycle life, SB plays an important role while calendaring is detrimental to electrochemical behaviour. Long cycle life is only achieved for non-calendared electrodes with high SB loading which results in lower volumetric capacity than Graphite-based electrodes.

Acknowledgements

Financial support provided by the European Commission (EC), through the project EuroLiion (NMP3-SL-2010-265368) is gratefully acknowledged.

References

[1] T. Tran, J. Feikert, X. Song, K. Kinosbita, J. Electrochem. Soc. 142 (1995) 3297.
[2] M.N. Obrovac, L. Christensen, Electrochem. Solid State Lett. 7 (2004) A93.
[3] J.H. Ryu, J.W. Kim, Y.-E. Sung, S.M. Oh, Electrochem. Solid State Lett. 7 (2004) A306.
[4] L.Y. Beaulieu, K.W. Eberman, R.L. Turner, L.J. Krause, J.R. Dahn, Electrochem. Solid State Lett. 4 (2001) A137.
[5] C.C. Nguyen, S.W. Song, Electrochim. Acta 55 (2010) 3026.
[6] L. Baggetto, R. Niessen, P. Notten, Electrochim. Acta 54 (2009) 5937.
[7] M. Winter, Z. Phys. Chem. 223 (2009) 1395.
[8] A. Magasinski, B. Zdyrko, I. Kovalenko, B. Hertzberg, R. Burtovyy, C.F. Huebner, T.F. Fuller, I. Luzinov, G. Yushin, J. Appl. Mater. Interfaces 2 (2010) 3004.
[9] B. Lestriez, C.R. Chimie 13 (2010) 1341.
[10] N.S. Hochgatterer, M.R. Schweiger, S. Koller, P.R. Raimann, T. Wohrle, C. Wurm, M. Winter, Electrochem. Solid State Lett. 11 (2008) A76.
[11] W.R. Liu, M.H. Yang, H.C. Wu, S.M. Chiao, N.L. Wu, Electrochem. Solid State Lett. 8 (2005) A100.
[12] H. Buqa, M. Holzapfel, F. Krumeich, C. Veit, P. Novak, J. Power Sources 161 (2006) 617.
[13] J. Li, R.B. Lewis, J.R. Dahn, Electrochem. Solid State Lett. 10 (2007) A17.
[14] B. Lestriez, S. Bahri, I. Sandu, L. Roué, D. Guyomard, Electrochem. Commun. 9 (2007) 2801.
[15] I. Kovalenko, B. Zdyrko, A. Magasinski, B. Hertzberg, Z. Milicev, R. Burtovyy, I. Luzinov, G. Yushin, Science 334 (2011) 75.
[16] B. Koo, H. Kim, Y. Cho, K.T. Lee, N.-S. Choi, J. Cho, Angew. Chem. Int. Ed. 51 (2012) 8762.
[17] Z.-J. Han, N. Yabuuchi, K. Shimomura, M. Murase, H. Yui, S. Komaba, Energy Environ. Sci. 5 (2012) 9014.
[18] M.-H. Ryou, J. Kim, I. Lee, S. Kim, Y.K. Jeong, S. Hong, J.H. Ryu, T.-S. Kim, J.-K. Park, H. Lee, J.W. Choi, Adv. Mater. 25 (2013) 1571.
[19] M. Ulldemolins, F. Le Cras, B. Pecquenard, V.P. Phan, L. Martin, H. Martinez, J. Power Sources 206 (2012) 245.
[20] H. Nakai, T. Kubota, A. Kita, A. Kawashima, J. Electrochem. Soc. 158 (2011) A798.
[21] N.-S. Choi, K.H. Yew, K.Y. Lee, M.S. Sung, S.-S. Kim, J. Power Sources 161 (2006) 1254.
[22] N.-S. Choi, Y. Lee, S. Kim, S.-C. Shin, Y.-M. Kang, J. Power Sources 195 (2010) 2368.
[23] L. Chen, K. Wang, X. Xie, J. Xie, J. Power Sources 174 (2007) 538.
[24] R.R. Garsuch, D.-B. Le, A. Garsuch, J. Li, S. Wang, A. Farooq, J.R. Dahn, J. Electrochem. Soc. 155 (2008) A721.
[25] D. Mazouzi, N. Delpuech, Y. Oumellal, M. Gauthier, M. Cerbelaud, J. Gaubicher, N. Dupré, P. Moreau, D. Guyomard, L. Roué, B. Lestriez, J. Power Sources 220 (2012) 180.
[26] V. Etacheri, O. Haik, Y. Goffer, G.A. Roberts, I.C. Stefan, R. Fasching, D. Aurbach, Langmuir 28 (2012) 965.
[27] B. Lestriez, S. Desaever, J. Danet, P. Moreau, D. Plée, D. Guyomard, Electrochem. Solid State Lett. 12 (2009) A76.
[28] B.P.N. Nguyen, N.A. Kumar, J. Gaubicher, F. Duclairoir, T. Brousse, O. Crosnier, L. Dubois, G. Bidan, D. Guyomard, B. Lestriez, Adv. Energy Mater. 3 (2013) 1351.
[29] B.P.N. Nguyen, J. Gaubicher, B. Lestriez, http://dx.doi.org/10.1016/j.electacta.2013.12.126.
[30] D. Mazouzi, B. Lestriez, L. Roué, D. Guyomard, Electrochem. Solid State Lett. 12 (2009) A215.
[31] M. Cerbelaud, B. Lestriez, D. Guyomard, A. Videcoq, R. Ferrando, Langmuir 28 (2012) 10713.
[32] C.C. Li, X. Peng, J. Lee, F. Wang, J. Electrochem. Soc. 157 (2010) A517.
[33] C.C. Li, Y. Wang, T. Yang, J. Electrochem. Soc. 158 (2011) A828.
[34] J. Li, B. Armstrong, J. Kiggans, C. Daniel, D. Wood, Langmuir 28 (2012) 3783.
[35] W. Porcher, B. Lestriez, S. Jouanneau, D. Guyomard, J. Power Sources 195 (2010) 2835.
[36] C.-C. Chang, L.-J. Her, H.-K. Su, S.-H. Hsu, Y. Te Yen, J. Electrochem. Soc. 158 (2011) A481.
[37] C.C. Li, J. Lee, C. Lo, M. Wu, Electrochem. Solid State Lett. 8 (2005) A509.
[38] C.C. Li, J. Lee, X. Peng, J. Electrochem. Soc. 153 (2006) A809.
[39] T.J. Patey, A. Hintennach, F. La Mantia, P. Novák, J. Power Sources 189 (2009) 590.
[40] W.B. Russel, D.A. Saville, W.R. Schowalter, Colloidal Dispersions, second ed., Cambridge University Press, Cambridge, 1991.
[41] R. Hunter, Foundations of Colloid Science, vol. I, Clarendon Press, Oxford, 1992.
[42] J. Israelachvili, Intermolecular and Surface Forces, third ed., Academic Press, London, 1997.
[43] J.-H. Lee, U. Paik, V.A. Hackley, Y.-M. Choi, J. Electrochem. Soc. 152 (2005) A1763.
[44] M. Pawlik, Colloids Surf. A 266 (2005) 82.
[45] T. Ueno, S. Yokota, T. Kitaoka, H. Wariishi, Carbohydr. Res. 342 (2007) 2593.
[46] R.A. Jones, R.W. Richards, Polymers at Surfaces and Interfaces, Cambridge University Press, New York, 1999.
[47] M.N. Obrovac, L.J. Krause, J. Electrochem. Soc. 154 (2007) A103.
[48] Y. Oumellal, N. Delpuech, D. Mazouzi, N. Dupré, J. Gaubicher, P. Moreau, P. Soudan, B. Lestriez, D. Guyomard, J. Mater. Chem. 21 (2011) 6201.
[49] N. Delpuech, N. Dupré, D. Mazouzi, J. Gaubicher, P. Moreau, J.S. Bridel, D. Guyomard, B. Lestriez, Electrochem. Commun. 33 (2013) 72.
[50] W. Porcher, B. Lestriez, S. Jouanneau, D. Guyomard, J. Electrochem. Soc. 156 (2009) A133.
[51] J.H. Lee, U. Paik, V.A. Hackley, Y.M. Choi, J. Electrochem. Soc. 152 (2005) 1763.
[52] J.H. Lee, S. Lee, U. Paik, Y.M. Choi, J. Power Sources 147 (2005) 249.
[53] A. Guerfi, M. Kaneko, M. Petitclerc, M. Mori, K. Zaghib, J. Power Sources 163 (2007) 1047.
[54] C.-C. Li, Y.-S. Lin, J. Power Sources 220 (2012) 413.
[55] C.-C. Li, Y.-W. Wang, J. Electrochem. Soc. 158 (2011) A1361.
[56] S. Lim, K.H. Ahn, M. Yamamura, Langmuir 29 (2013) 8233.
[57] D. Reyter, S. Rousselot, D. Mazouzi, M. Gauthier, P. Moreau, B. Lestriez, D. Guyomard, L. Roué, J. Power Sources 239 (2013) 308.
[58] S.D. Beattie, D. Larcher, M. Morcrette, B. Simon, J.-M. Tarascon, J. Electrochem. Soc. 155 (2008) A158.